Noninvasive Vascular Imaging of Polypoidal Choroidal Vasculopathy by Doppler Optical Coherence Tomography

Masahiro Miura,[1,2] Daisuke Muramatsu,[1,2] Young-Joo Hong,[3] Yoshiaki Yasuno,[3] Takuya Iwasaki,[1,2] and Hiroshi Goto[2]

[1]Department of Ophthalmology, Tokyo Medical University, Ibaraki Medical Centre, Ami, Japan

[2]Department of Ophthalmology, Tokyo Medical University, Tokyo, Japan

[3]Computational Optics Group, University of Tsukuba, Tsukuba, Japan

Correspondence:

Masahiro Miura, MD, PhD

Department of Ophthalmology, Tokyo Medical University, Ibaraki Medical Centre

3-20-1 Chuo, Ami, Inashiki, Ibaraki 3000395, Japan

Phone: +81-298-87-1161 Fax: +81-298-87-7656 E-mail: m-miura@tokyo-med.ac.jp

Word count

Title: 12 words, Abstract: 238 words, Text: 2452 words, 7 Figures

Grant

This project was supported in part by KAKENHI (24592682) and the Japan Science and Technology Agency through a program of the Development of Systems and Technology for Advanced Measurement and Analysis.

Keywords: polypoidal choroidal vasculopathy, optical coherence tomography, Doppler, OCT angiography, polypoidal lesion

Abstract

Purpose

To noninvasively investigate the vascular architecture of polypoidal lesions in polypoidal choroidal vasculopathy (PCV) using Doppler optical coherence tomography (OCT), and to evaluate the clinical usefulness of Doppler OCT for the assessment of therapeutic effects in PCV.

Methods

Fifteen eyes of 15 patients with treatment-naïve PCV were prospectively studied. Vascular imaging was obtained using 1,060-nm swept-source Doppler OCT, and compared with indocyanine green angiography (ICGA) images. The therapeutic effect of three consecutive intravitreal aflibercept injections was evaluated with ICGA and Doppler OCT.

Results

In Doppler OCT images, polypoidal lesions were clearly detected at the corresponding locations of lesions in the ICGA images. By being insensitive to dye leakage, Doppler OCT identified the complicated vascular structure in the polypoidal lesions. The identified mean area of the polypoidal lesions in the Doppler OCT images (0.04 mm^2) was significantly smaller than that of the ICGA images (0.13 mm^2). Polypoidal lesions were located in the retinal pigment epithelial detachment in 13 eyes, in the choroid in one eye, and in both the retinal pigment epithelial detachment and choroid in one eye. After intravitreal aflibercept treatment, areas of polypoidal lesions in the ICGA images were decreased in 14 of 15 eyes. This therapeutic effect was clearly confirmed in the Doppler OCT images.

Conclusions

Doppler OCT imaging clearly detected fine vascular structures at the polypoidal lesions in PCV. Doppler OCT might be useful for the diagnosis and evaluation of therapeutic effects in PCV.

Polypoidal choroidal vasculopathy (PCV) is a variation of age-related macular degeneration and is characterized by numerous recurrent, bilateral, asymmetric, serosanguinous detachments in the retinal pigment epithelium.[1] In indocyanine green angiography (ICGA) imaging, polypoidal vascular lesions and a branching vascular network were described as characteristic findings in PCV.[2,3] Despite a number of clinical studies, the origin and location of these vascular lesions are still controversial.[3] Some studies speculated vascular lesions were located in the subretinal pigment epithelium (sub-RPE) and represented a type of choroidal neovascularization.[4,5] Other studies, however, speculated that they were located in the inner choroid and represented pathological changes of the choroidal vessels.[6,7]

To clarify these speculations, evaluation of the three-dimensional (3-D) structure of PCV vascular lesions is crucial. In current clinical practice, the most reliable method to detect PCV vascular lesions is ICGA.[3] However, ICGA cannot evaluate the 3-D structure of PCV vascular lesions because of its poor axial resolution.[8] Optical coherence tomography (OCT) has achieved micrometer-level axial resolution in cross-sectional retinal imaging,[9] and provided important information about the 3-D retinal structure in PCV.[10-12] However, standard OCT is only sensitive to backscattered light intensity and cannot provide information about blood flow. Because of this limitation, standard OCT has a limited ability to evaluate PCV vascular lesions.

Recently, a functional extension of OCT technology for 3-D vascular imaging was developed. This technique was first reported using Doppler OCT and was named optical coherence angiography.[13] Following this development, various 3-D vascular imaging techniques were reported,[14-22] and were collectively called OCT angiography. In the previous studies for PCV with OCT angiography, 3-D architectures of the branching vascular networks were evaluated and their presence in the sub-RPE space was reported.[14,15,23] However, these studies did not evaluate the polypoidal lesions,[14,15,23] despite polypoidal lesions being a representative finding of PCV.[2,3] Polypoidal lesions are a crucial finding for the diagnosis and treatment of PCV,[2,3] hence investigation of its 3-D structure might provide important information about the pathophysiology and treatment strategy for PCV. In this paper, we evaluate the

3-D vascular architecture of polypoidal lesions in PCV using Doppler OCT, and describe the clinical usefulness of Doppler OCT for PCV.

Methods

We prospectively evaluated 15 eyes of 15 Japanese patients with treatment-naïve PCV (13 male, two female; age range, 51–83 years; mean age, 68.5 years). The clinical diagnosis of PCV was made by identification of polypoidal lesions with ICGA. Eyes with a history of treatment for PCV or age-related macular degeneration were excluded. Eyes with severe cataracts or other eye diseases that interfered with Doppler OCT image quality were excluded from this study. All eyes were treated with intravitreal injections of 2.0 mg aflibercept (Eylea; Regeneron, Tarrytown, PA, USA and Bayer Health Care, Berlin, Germany) every 4 weeks. Both ICGA imaging and Doppler OCT imaging were performed on each patient before and after three consecutive intravitreal aflibercept treatments. ICGA imaging was performed using a confocal scanning laser ophthalmoscope (F-10; Nidek, Gamagori, Japan).

The Doppler OCT system used in this study was a custom-made prototype built by the Computational Optic Group at the University of Tsukuba.[16,22,23] This Doppler OCT was based on swept-source OCT technology, and operated at an axial scan speed of 100,000 A-scans/s, using a swept-source laser at a central wavelength of 1,060 nm. The probing beam power was set at 1.85 mW, which is lower than the American National Standards Institute safety limit. The axial resolution for the tissue in this study was 6.4 μm. The Doppler signal was calculated from two A-lines in two successive B-scans. Doppler signals were displayed in the form of the squared energy of the Doppler phase shift. No thresholds were applied to Doppler signals for imaging analysis. A raster scanning protocol with 256 A-lines × 2,048 B-scans covering a 1.5 × 1.5-mm region on the retina was used for volumetric scans. The acquisition speed of each measurement was 6.6 s/volume. In a single volume scan, the system simultaneously provided both an intensity-based standard OCT image volume and a Doppler OCT image volume. Composite color Doppler OCT images, in which the Doppler OCT signal was overlaid on the standard OCT with purple color, were created from standard OCT and Doppler OCT images to specify the location of blood flow in the standard OCT image. For *en face* Doppler images, we segmented retinal surfaces and RPE layers based on the standard OCT image, and the *en face* projection of the Doppler

OCT was created using the depth range from the retinal surface to 1 mm below the RPE layer. To present detailed features in a print format, the *en face* projection images in figures were processed by convolution filtering software (ImageJ, ver. 1.47, National Institute of Health, Bethesda, MD, USA) and contrast and brightness adjustment software (Adobe Photoshop CS5, Adobe Systems, San Jose, CA, USA) (Fig. 1). However, all evaluations in the study were performed with unprocessed images, so the study result was not affected by filtering and contrast corrections.

To evaluate the therapeutic effects, the reduction rates of polypoidal lesions in the late phase of ICCA images and *en face* Doppler OCT images were calculated using the following formula:

$$\text{Reduction rate} = \left(1 - \frac{\text{area after treatment}}{\text{area before treatment}}\right) \times 100$$

The areas of polypoidal lesions in ICGA images were calculated using a built-in program of the scanning laser ophthalmoscope (F-10), and the area in the *en face* Doppler OCT image was calculated using image analysis software (ImageJ, ver. 1.47). Contours of polypoidal lesions were manually delineated for both ICGA and Doppler OCT by a retina specialist (M.M.). For *en face* Doppler OCT images, unprocessed images were used for the computations.

This study was performed according to the tenets of the Declaration of Helsinki, and was approved by the Institutional Review Boards of the University of Tsukuba and Tokyo Medical University. Informed consent for the study was obtained from all participants.

Results

Polypoidal lesions were detected in the late phase of ICGA in all 15 eyes, and feeder vessels to polypoidal lesions were detected in four eyes in the early phase of ICGA (Figs. 2A, 5A). *En face* projection images of Doppler OCT images clearly showed polypoidal lesions at the corresponding locations of lesions in the ICGA images (Figs. 2D, 3D, 4D, 5D). Topographical locations of polypoidal lesions were readily determined by Doppler OCT B-scan images (Figs. 2F, 3F, 4F, 5F). Polypoidal lesions were located in the pigment epithelial detachment in 13 eyes (Figs. 2F, 3F), in the choroid in one eye (Fig. 4F), and in both the pigment epithelial detachment and the choroid in one eye (Fig. 5F). In the eyes with feeder vessels, polypoidal lesions were located in the sub-RPE space in three eyes (Fig. 2F) and both the sub-RPE space and choroid in one eye (Fig. 5F). In the other 11 eyes without feeder vessels, polypoidal lesions were located in the sub-RPE space in 10 eyes (Fig. 3F) and the inner choroid in one eye (Fig. 4F). In standard OCT B-scan images, polypoidal lesions were displayed as high-intensity areas, and low-intensity areas in the polypoidal lesions were occasionally detected (Fig. 3E). In contrast to Doppler OCT, localization of polypoidal lesions in standard OCT B-scan images was difficult because of the poor discrimination ability from the surrounding tissues (Figs. 2E, 3E, 4E, 5E).

In the late phase of ICGA images, polypoidal lesions were delineated as homogeneous hyperfluorescent areas in all eyes, and multiple lobules in the polypoidal lesions in the early phase of ICGA images (Fig. 5A) were detected in three eyes. In contrast to the ICGA images, *en face* projection images of Doppler OCT showed more complicated vascular structures at the polypoidal lesions. In seven of 15 eyes, each polypoidal lesion in an ICGA image consisted of multiple polypoidal lesions in Doppler OCT images (Figs. 2D, 5D). In six of 15 eyes, Doppler OCT showed a fine vascular network in the polypoidal lesions. In these eyes, polypoidal lesions were delineated as focal aneurysmal dilations in the vascular network (Fig. 2D). Fine vascular structures at the feeder vessels were clearly detected (Fig. 2D) in the Doppler OCT images. In one eye, some polypoidal lesions in the early phase of the ICGA images were less clear in the late phase, and Doppler OCT imaging clearly detected these polypoidal lesions

(Fig. 3D). The mean of the total area of polypoidal lesions was 0.13 mm^2 [standard deviation (SD): 0.094] in the late phase of ICGA images and 0.04 mm^2 (SD: 0.030) in the *en face* projection images of Doppler OCT. The mean of the total area in the ICGA images was significantly larger than the Doppler OCT images (P = 0.0007, Wilcoxon signed rank test, Fig. 6).

After intravitreal aflibercept treatment, areas of polypoidal lesions in the ICGA images were decreased in 14 of 15 eyes. *En face* projection images of Doppler OCT clearly detected this therapeutic effect (Figs. 3G, 4G, 5G). The mean of the total area of polypoidal lesions was decreased from 0.13 mm^2 (SD: 0.094) to 0.056 mm^2 (SD: 0.086) in the late phase of the ICGA images, and from 0.04 mm^2 (SD: 0.03) to 0.017 mm^2 (SD: 0.024) in the Doppler OCT images. The area of polypoidal lesions was significantly decreased in both ICGA and Doppler OCT images (P = 0.007 in both ICGA and Doppler OCT, Wilcoxon signed rank test). The mean reduction rate was 65.8% (SD: 38.1) in the ICGA images and 66.6% (SD: 35.0) in the Doppler OCT images. The reduction rate in the Doppler OCT images was significantly correlated with the ICGA images (R^2 = 0.82, P = 0.0007, Fig. 7).

Discussion

In the present study, we used Doppler OCT to investigate the vascular architecture at polypoidal lesions in PCV. In ICGA images, evaluation of fine microvascular structures at the polypoidal lesions was significantly impeded by dye leakage from the vascular lesions. Doppler OCT imaging was insensitive to leakage from abnormal vessels and could provide detailed information about the microvascular structure at the polypoidal lesions. From Doppler OCT findings, polypoidal lesions consisted of a microvascular network with focal aneurysmal dilatation. This finding was in good agreement with previous histopathological studies.[24,25] The area of the polypoidal lesions in the ICGA images was three times larger than in the Doppler OCT images, and this finding might represent the degree of leakage from polypoidal lesions. Some polypoidal lesions in the early phase of ICGA and Doppler OCT images became unclear in the late phase of ICGA images, which might represent low activity at these polypoidal lesions. Comparison between Doppler OCT images and ICGA images might be useful as an index parameter of the activity of the lesion.

There have been several studies of the topographical locations of polypoidal lesions using standard OCT and ICGA. Some studies speculated that the lesions were located in the sub-RPE space,[4,5,11,12] whereas others speculated that they were located at the inner choroid.[26] In the studies with *en face* swept-source OCT imaging, vascular abnormalities were located either above or below Bruch's membrane.[27,28] Standard OCT and ICGA have a limited ability to evaluate topographic locations of vascular lesions, and this limitation impedes a definitive conclusion about the topographic location of the polypoidal lesions. In this study, Doppler OCT imaging could readily determine the topographic location of polypoidal lesions. Polypoidal lesions were located in the sub-RPE space or inner choroid or both inner choroid and sub-RPE space. This result suggested diversity of the topographic locations of the polypoidal lesions. In previous studies, abnormal vessels in PCV were thought to penetrate Bruch's membrane from the inner choroid and distribute into the sub-RPE space.[5,10,14,15,23,29] This study showed that polypoidal lesions could be developed either before or after penetration of Bruch's membrane. This

diversity might address the previous controversy over the topographic location of polypoidal lesions.

Some studies have attempted to classify PCV vascular lesions by the presence of feeder vessels, and reported their association with therapeutic effects.[30,31] Kawamura et al. reported vascular lesions with feeder vessels (type 1 PCV) located in the sub-RPE space, and vascular lesions without feeder vessels (type 2 PCV) were located in the inner choroid.[31] In our case series, polypoidal lesions were located in either the inner choroid or sub-RPE space despite the presence of feeder vessels. It is unreasonable to make a definitive conclusion with a small number of cases; however, in the present study, the presence of feeder vessels did not have an absolute relationship with the topographic locations of polypoidal lesions.

In our case series, a decrease in the polypoidal lesions in ICGA images after three consecutive intravitreal aflibercept treatments was detected in 14 of 15 eyes (93%). Doppler OCT clearly detected this reduction in the polypoidal lesions and could be used as a noninvasive alternative method to evaluate the therapeutic effect on polypoidal lesions. In one case of our study, polypoidal lesions in the sub-RPE space showed a better response to intravitreal aflibercept treatment than the lesions in the choroid (Fig. 4). The therapeutic effect of choroidal neovascularization after intravitreal ranibizumab treatment was influenced by their topographical location,[32] and the topographic locations of polypoidal lesions in PCV might also be related to the therapeutic effects. Further study is required to evaluate the clinical significance of the topographical locations of polypoidal lesions.

The current study had several limitations. Some areas of PCV vascular lesions might have been missed even with highly sensitive Doppler measurements. With the small number of subjects in our case series, this study evaluated only some of the variations in PCV. The small measurement area of Doppler OCT impeded evaluation of the entire structure of PCV vascular lesions. In the present study, 6.6 seconds were required for a single measurement, despite using high-speed 100 kHz OCT. Longer measurement times are required for wide measurement areas, and might cause motion artifacts in vascular imaging. A motion correction algorithm using orthogonal scan patterns might be a possible

solution.[33] Another possible solution would be using ultra-high-speed OCT to shorten the measurement times. Vascular imaging with ultra-high-speed OCT has already been reported,[34,35] indicating the influence of motion artifacts could be compensated by shortened measurement times.

In conclusion, this study demonstrated the clinical utility of Doppler OCT to evaluate PCV vascular lesions. Doppler OCT could detect only some parts of the choroidal vasculature; hence, ICGA is still required to more thoroughly evaluate the entire structure of vascular lesions. Doppler OCT cannot detect dye leakage in fluorescein angiography, and dye leakage is an important indicator of the activity of polypoidal lesions. However, the clinical applications of ICGA and fluorescein angiography have been limited because of patient discomfort and relatively long measurement times. Doppler OCT imaging is noninvasive, has a short measurement time, and may potentially function as a noninvasive alternative to fluorescein angiography and ICGA for the assessment of PCV.

References

1. Yannuzzi LA, Sorenson J, Spaide RF, Lipson B. Idiopathic polypoidal choroidal vasculopathy (IPCV). *Retina.* 1990;10:1-8.

2. Spaide RF, Yannuzzi LA, Slakter JS, Sorenson J, Orlach DA. Indocyanine green videoangiography of idiopathic polypoidal choroidal vasculopathy. *Retina.* 1995;15:100-110.

3. Lim TH, Laude A, Tan CS. Polypoidal choroidal vasculopathy: an angiographic discussion. *Eye.* 2010;24:483-490.

4. Costa RA, Navajas EV, Farah ME, Calucci D, Cardillo JA, Scott IU. Polypoidal choroidal vasculopathy: angiographic characterization of the network vascular elements and a new treatment paradigm. *Prog Retin Eye Res.* 2005;24:560-586.

5. Tsujikawa A, Sasahara M, Otani A, et al. Pigment epithelial detachment in polypoidal choroidal vasculopathy. *Am J Ophthalmol.* 2007;143:102-111.

6. Nakashizuka H, Mitsumata M, Okisaka S, et al. Clinicopathologic findings in polypoidal choroidal vasculopathy. *Invest Ophthalmol Vis Sci.* 2008;49:4729-4737.

7. Yuzawa M, Mori R, Kawamura A. The origins of polypoidal choroidal vasculopathy. *Br J Ophthalmol.* 2005;89:602-607.

8. Bartsch DU, Freeman WR. Axial intensity distribution analysis of the human retina with a confocal scanning laser tomograph. *Exp Eye Res.* 1994;58:161-173.

9. Huang D, Swanson E, Lin C, et al. Optical coherence tomography. *Science.* 1991;254:1178-1181.

10. Ojima Y, Hangai M, Sakamoto A, et al. Improved visualization of polypoidal choroidal vasculopathy lesions using spectral-domain optical coherence tomography. *Retina.* 2009;29:52-59.

11. Yasuno Y, Miura M, Kawana K, et al. Visualization of sub-retinal pigment epithelium morphologies of exudative macular diseases by high-penetration optical coherence tomography. *Invest Ophthalmol Vis Sci.* 2009;50:405-413.

12. Nagase S, Miura M, Makita S, Iwasaki T, Goto H, Yasuno Y. High-penetration optical coherence tomography with enhanced depth imaging of polypoidal choroidal vasculopathy. *Ophthalmic Surg Lasers Imaging.* 2012;43: e5-9.

13. Makita S, Hong Y, Yamanari M, Yatagai T, Yasuno Y. Optical coherence angiography. *Opt Express.* 2006;14:7821-7840.

14. Miura M, Makita S, Iwasaki T, Yasuno Y. Three-dimensional visualization of ocular vascular pathology by optical coherence angiography in vivo. *Invest Ophthalmol Vis Sci.* 2011;52:2689-2695.

15. Makita S, Jaillon F, Yamanari M, Miura M, Yasuno Y. Comprehensive in vivo micro-vascular imaging of the human eye by dual-beam-scan Doppler optical coherence angiography. *Opt Express.* 2011;19:1271-1283.

16. Hong YJ, Makita S, Jaillon F, et al. High-penetration swept source Doppler optical coherence angiography by fully numerical phase stabilization. *Opt Express.* 2012;20:2740-2760.

17. Szkulmowska A, Szkulmowski M, Szlag D, Kowalczyk A, Wojtkowski M. Three-dimensional quantitative imaging of retinal and choroidal blood flow velocity using joint Spectral and Time domain Optical Coherence Tomography. *Opt Express.* 2009;17:10584-10598.

18. An L, Wang RK. In vivo volumetric imaging of vascular perfusion within human retina and choroids with optical micro-angiography. *Opt Express.* 2008;16:11438-11452.

19. Schwartz DM, Fingler J, Kim DY, et al. Phase-variance optical coherence tomography: a technique for noninvasive angiography. *Ophthalmology.* 2014;121:180-187.

20. Mariampillai A, Leung MK, Jarvi M, et al. Optimized speckle variance OCT imaging of microvasculature. *Opt Lett.* 2010;35:1257-1259.

21. Jia Y, Tan O, Tokayer J, et al. Split-spectrum amplitude-decorrelation angiography with optical coherence tomography. *Opt Express.* 2012;20:4710-4725.

22. Miura M, Hong Y, Yasuno Y, Muramatsu D, Iwasaki T, Goto H. Three-dimensional Vascular Imaging of Proliferative Diabetic Retinopathy by Doppler Optical Coherence Tomography. *Am J*

Ophthalmol. 2015;159:528-538.

23. Hong YJ, Miura M, Makita S, et al. Noninvasive investigation of deep vascular pathologies of exudative macular diseases by high-penetration optical coherence angiography. *Invest Ophthalmol Vis Sci.* 2013;54:3621-3631.

24. Lafaut BA, Aisenbrey S, Van den Broecke C, Bartz-Schmidt KU, Heimann K. Polypoidal choroidal vasculopathy pattern in age-related macular degeneration: a clinicopathologic correlation. *Retina.* 2000;20:650-654.

25. Okubo A, Sameshima M, Uemura A, Kanda S, Ohba N. Clinicopathological correlation of polypoidal choroidal vasculopathy revealed by ultrastructural study. *Br J Ophthalmol.* 2002;86:1093-1098.

26. Iijima H, Imai M, Gohdo T, Tsukahara S. Optical coherence tomography of idiopathic polypoidal choroidal vasculopathy. *Am J Ophthalmol.* 1999;127:301-305.

27. Alasil T, Ferrara D, Adhi M, et al. En Face Imaging of the Choroid in Polypoidal Choroidal Vasculopathy Using Swept-Source Optical Coherence Tomography. *Am J Ophthalmol.*, in press. doi 10.1016/j.ajo.2014.12.012.

28. Sayanagi K, Gomi F, Akiba M, Sawa M, Hara C, Nishida K. En-face high-penetration optical coherence tomography imaging in polypoidal choroidal vasculopathy. *Br J Ophthalmol.* 2015;99:29-35.

29. Kim JH, Kang SW, Kim TH, Kim SJ, Ahn J. Structure of polypoidal choroidal vasculopathy studied by colocalization between tomographic and angiographic lesions. *Am J Ophthalmol.* 2013;156:974-980.

30. Tan C, Ngo WK, Lim LW, Lim TH. A novel classification of the vascular patterns of polypoidal choroidal vasculopathy and its relation to clinical outcomes. *Br J Ophthalmol.* 2014;98:1528-1533.

31. Kawamura A, Yuzawa M, Mori R, Haruyama M, Tanaka K. Indocyanine green angiographic and optical coherence tomographic findings support classification of polypoidal choroidal vasculopathy

into two types. *Acta Ophthalmol.* 2013;91:e474-481.

32. Framme C, Panagakis G, Birngruber R. Effects on choroidal neovascularization after anti-VEGF upload using intravitreal ranibizumab, as determined by spectral domain-optical coherence tomography. *Invest Ophthalmol Vis Sci.* 2010;51:1671-1676.

33. Kraus MF, Potsaid B, Mayer MA, et al. Motion correction in optical coherence tomography volumes on a per A-scan basis using orthogonal scan patterns. *Biomed Opt Express.* 2012;3:1182-1199.

34. Blatter C, Klein T, Grajciar B, et al. Ultrahigh-speed non-invasive widefield angiography. *J Biomed Opt.* 2012;17:070505.

35. Choi W, Mohler KJ, Potsaid B, et al. Choriocapillaris and choroidal microvasculature imaging with ultrahigh speed OCT angiography. *PLoS One.* 2013;8:e81499.

Figure Legends

Figure 1. Image processing for *en face* projection of Doppler OCT images for better visualization in the print format. **(A)** Original image. **(B)** Image after application of convolution filter and adjustment of brightness and contrast.

Figure 2. ICGA and Doppler OCT images of PCV obtained from the left eye of a 70-year-old male. The late phase of the ICGA image **(B)** shows polypoidal lesions on the macula. The early phase of the ICGA image **(A)** shows feeder vessels of polypoidal lesions (yellow arrow). The late phase of the ICGA image after treatment shows no clear therapeutic effects for polypoidal lesions **(C)**. Yellow lines in the *en face* Doppler OCT images before **(D)** and after **(G)** treatment indicate the scanning line of B-scan OCT images before **(E, F)** and after **(H, I)** treatment, respectively. *En face* Doppler OCT image before treatment **(D)** clearly shows the vascular network with focal aneurysmal dilatation at polypoidal lesions. Standard OCT B-scan image before treatment **(E)** shows a high-intensity mass in the pigment epithelial detachment, and the composite Doppler OCT B-scan image **(F)** shows the presence of blood flow at polypoidal lesions (yellow arrow). After treatment, the *en face* Doppler OCT image **(G)**, standard OCT B-scan image **(H)**, and composite Doppler OCT B-scan image **(I)** show no clear therapeutic effects for polypoidal lesions.

Figure 3. ICGA and Doppler OCT images of PCV obtained from the left eye of a 72-year-old male. Early **(A)** and late phases **(B)** of the ICGA image before treatment show polypoidal lesions on the macula. The late phase of the ICGA image after treatment **(C)** shows disappearance of polypoidal lesions. Yellow lines in the *en face* Doppler OCT image before **(D)** and after **(G)** treatment indicate the scanning line of B-scan OCT images before **(E, F)** and after **(H, I)** treatment, respectively. *En face* Doppler OCT image before treatment **(D)** shows the polypoidal lesions at the corresponding locations of lesions in the ICGA images **(A)**. Some polypoidal lesions in the early phase of the ICGA image **(A)**

became unclear in the late phase (yellow arrow), and the Doppler OCT image **(D)** clearly detects these polypoidal lesions (yellow arrow). Standard OCT B-scan image before treatment **(E)** shows a high-intensity mass with a low-intensity (yellow arrow) area in the pigment epithelial detachment, and the composite Doppler OCT B-scan image **(F)** shows the presence of blood flow by the polypoidal lesions (yellow arrow). After treatment, an *en face* Doppler OCT image **(G)** and composite Doppler OCT B-scan image **(I)** show the disappearance of polypoidal lesions. Standard OCT B-scan image after treatment **(H)** shows the reduction of pigment epithelial detachment.

Figure 4. ICGA and Doppler OCT images of PCV obtained from the left eye of an 84-year-old male. Early **(A)** and late **(B)** phases of ICGA images before treatment show polypoidal lesions on the macula. The late phase of the ICGA images after treatment shows reduction of the lower part of the polypoidal lesions **(C)**. Yellow lines in the *en face* Doppler OCT image before **(D)** and after **(G)** treatment indicate the scanning line of B-scan OCT images before **(E, F)** and after **(H, I)** treatment, respectively. *En face* Doppler OCT image before treatment **(D)** shows the polypoidal lesion at the same location as in the ICGA images (yellow arrow). Standard OCT B-scan image before treatment **(E)** shows the pigment epithelial detachment. Composite Doppler OCT B-scan image **(F)** shows the presence of blood flow by the polypoidal lesion in the inner choroid (yellow arrow). After treatment, the *en face* Doppler OCT image **(G)** shows reduction of the lower part of the polypoidal lesion. Standard OCT B-scan image after treatment **(H)** shows reduction of the pigment epithelial detachment. Composite Doppler OCT B-scan image after treatment **(I)** shows the presence of a polypoidal lesion in the inner choroid (yellow arrow).

Figure 5. ICGA and Doppler OCT images of PCV obtained from the left eye of a 71-year-old female. The late phase of the ICGA image **(B)** before treatment shows a polypoidal lesion on the macula. The early phase of the ICGA image **(A)** shows multiple lobules in polypoidal lesions and feeder vessels (yellow arrow). The late phase of the ICGA image after treatment shows reduction of the polypoidal

lesions **(C)**. Yellow lines in the *en face* Doppler OCT image before **(D)** and after **(G)** treatment indicate the scanning line of the B-scan OCT images before **(E, F)** and after **(H, I)** treatment, respectively. *En face* Doppler OCT image before treatment **(D)** shows multiple lobules at the polypoidal lesion. Standard OCT B-scan image before treatment **(E)** shows a high-intensity mass in the pigment epithelial detachment. Composite Doppler OCT B-scan image **(F)** showing the presence of blood flow by polypoidal lesions in the inner choroid (white arrow) and pigment epithelial detachment (yellow arrow). After treatment, *en face* Doppler OCT image **(G)** shows reduction of the right part of the polypoidal lesion. Standard OCT B-scan image after treatment **(H)** shows pigment epithelial detachment. Composite Doppler OCT B-scan image after treatment **(I)** shows preservation of the polypoidal lesions in the inner choroid (white arrow) and disappearance of the polypoidal lesion in the pigment epithelial detachment.

Figure 6. Scatter plot of the total area of polypoidal lesions in ICGA and Doppler OCT images.

Figure 7. Scatter plot of the reduction rate of polypoidal lesions in ICGA and Doppler OCT images.

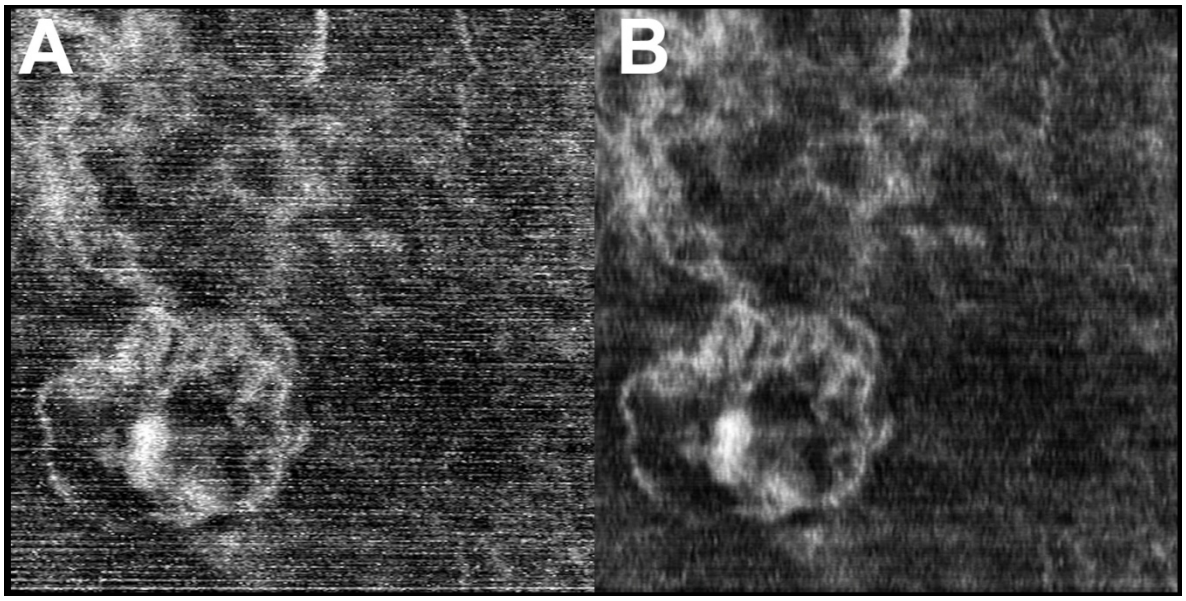

FIGURE 1

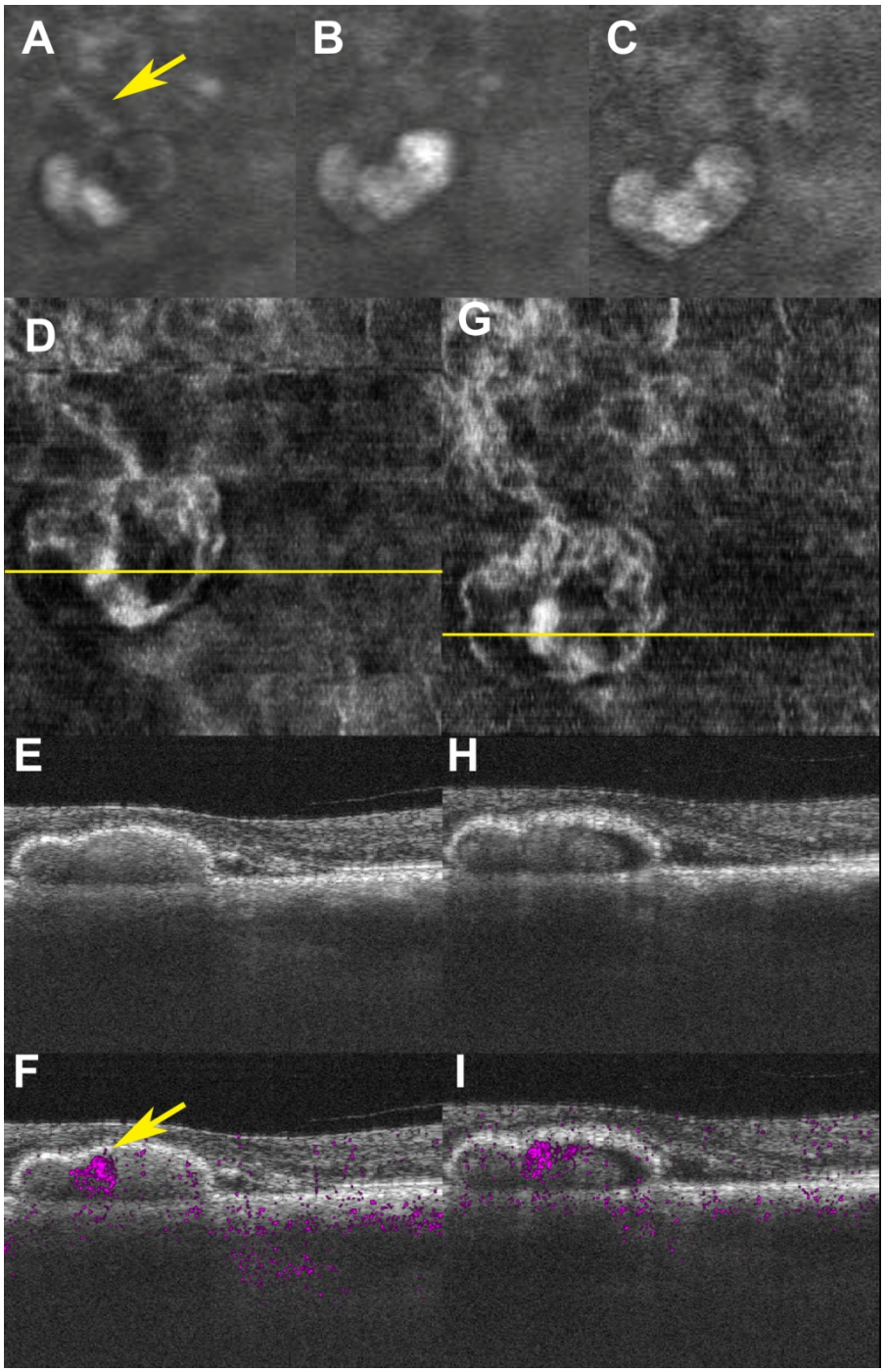

FIGURE 2

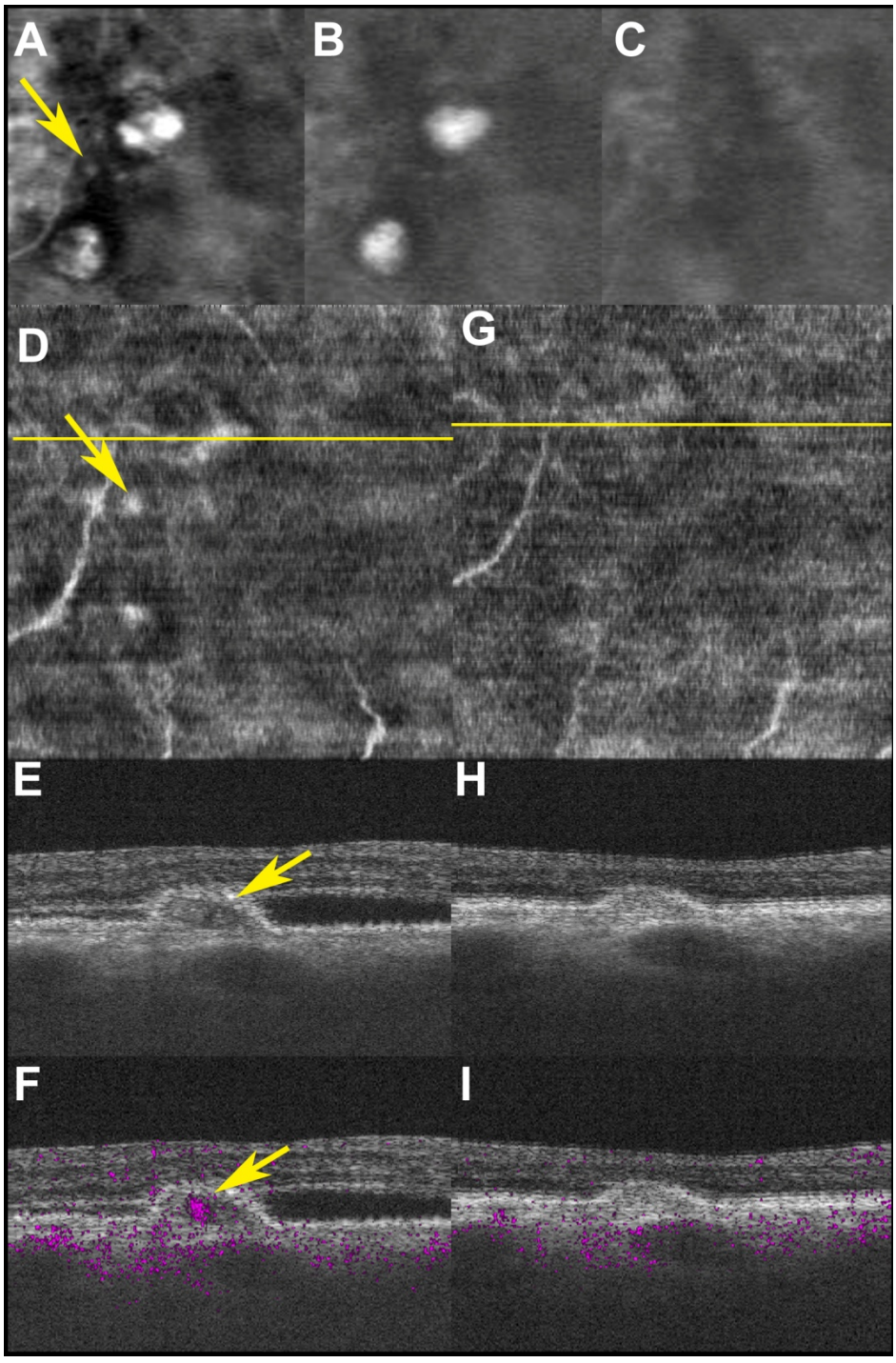

FIGURE 3

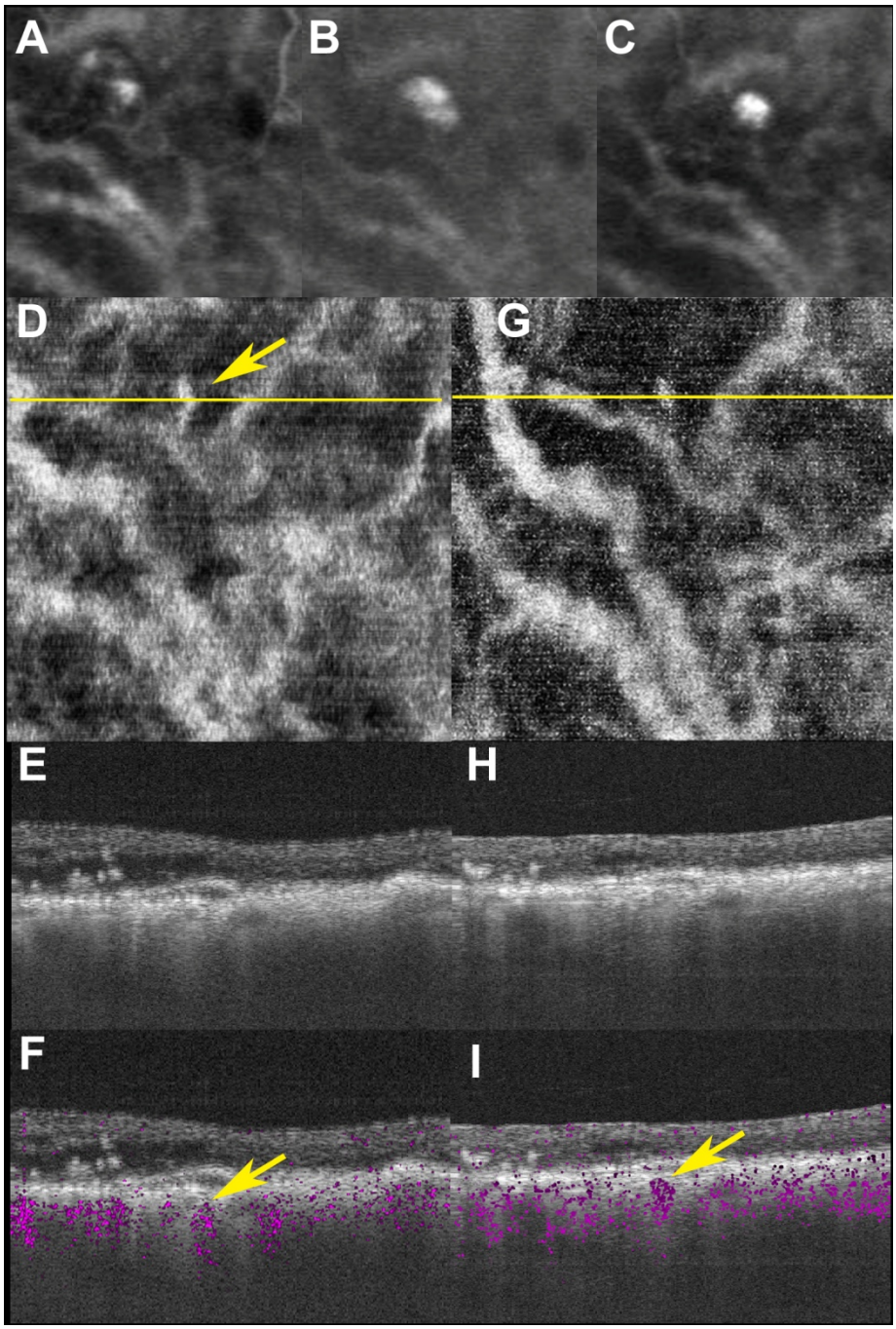

FIGURE 4

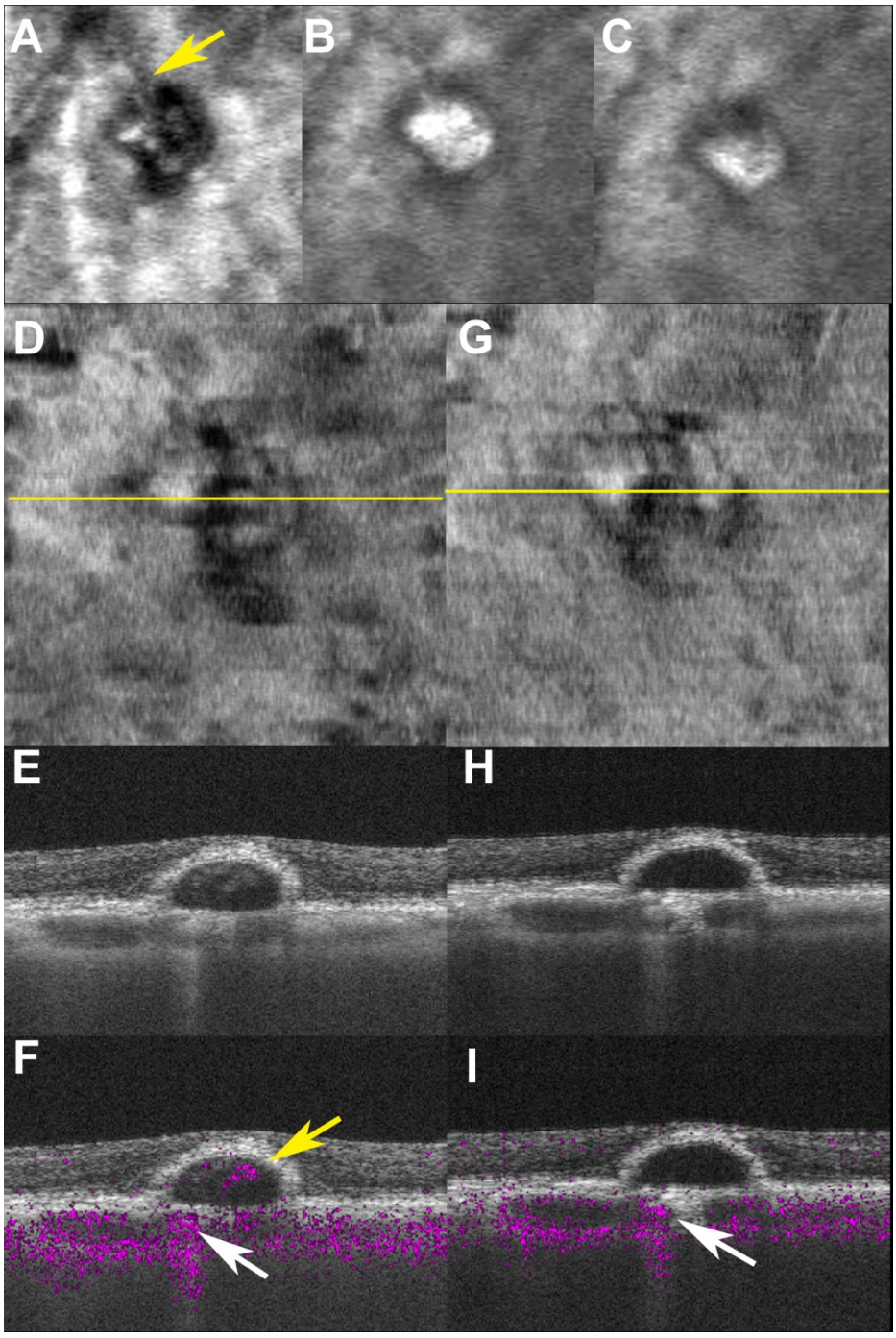

FIGURE 5

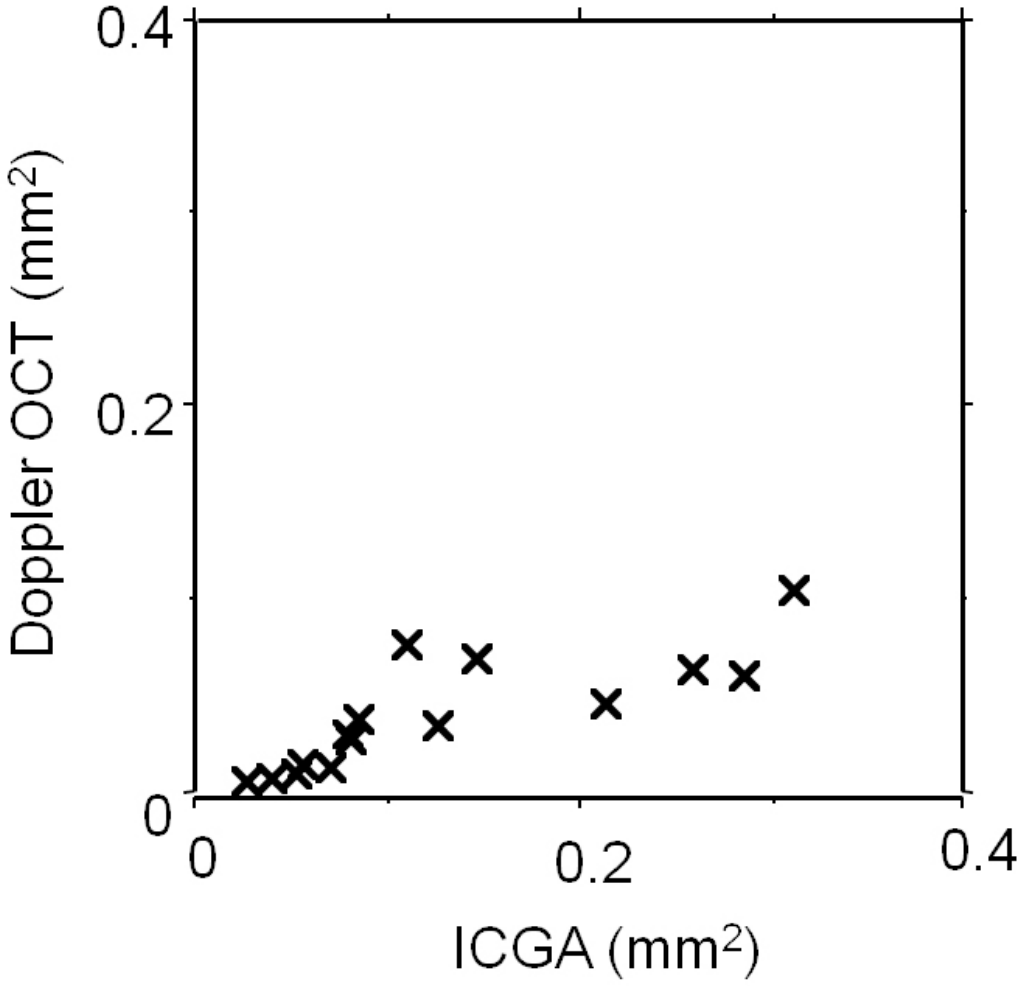

FIGURE 6

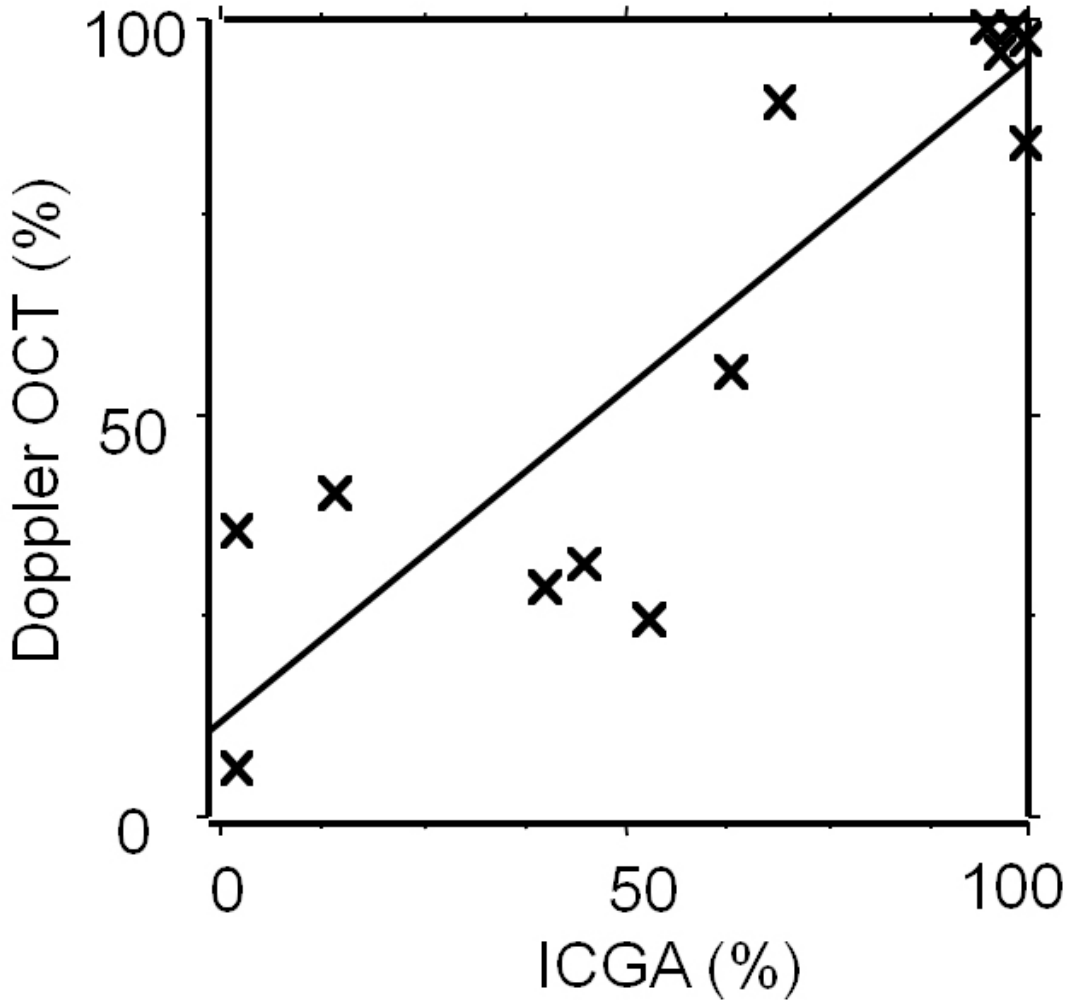

FIGURE 7